CHAPTER 2

Detection of Mercaptan Vapors Using Thin Films of Alkylamine-Passivated Gold Nanocrystals

ABSTRACT

Alkylamine-capped gold nanocrystals have been used as chemically sensitive resistors for the detection of volatile organic mercaptan vapors. Thin (< 1 x 10^{-4} cm) films of Au nanocrystals in the ≈ 7 nm size regime capped with dodecylamines were used to produce dc electrical resistances of (10 kΩ – 10 MΩ) when deposited onto interdigitated Au/Cr electrodes. These chemiresistive vapor detectors displayed a reversible increase in dc electrical resistance when exposed to non-thiol-containing organic vapors such as water, acetone, or toluene delivered at a constant fraction of their vapor pressure ($P/P^o = 0.050$), with $\Delta R/R_b$ responses to these vapors of typically only ≈ 5%. In contrast, the amine-capped Au nanocrystal films exhibited a much larger, irreversible, decrease in resistance upon exposure to vapors possessing the thiol (-SH) functionality, including H_2S, CH_3SH, and propanethiol. Optical spectroscopic data supports the hypothesis that the thiols displace the amine caps, allowing the gold cores to move closer and in some cases enter into contact, thereby lowering the film resistance. Consistently, the resistance of such films did not decrease upon exposure to octanethiol. At least for CH_3SH, the rate of resistance change under repeated experimental conditions allows extraction of the concentration of the thiol species over the range of 0.004–1.5 ppm in air.

I. INTRODUCTION

An important benchmark in the development of electronic olfaction is the successful reproduction of human nose detection thresholds and odor quality perceptions. Although tin-oxide [1] and MOSFET [2] sensors received early attention as artificial noses, much of the recent work in developing an electronic analog of mammalian olfaction has focused on sorption-based detectors, and such work is outlined in the introductory chapter of this thesis. A recent addition to the sorption-based detector approach utilizes organically capped gold nanocrystal films as an impedance read-out vapor sensor [3, 4]. In these detectors, analyte induced swelling of the organic cap layer moves neighboring particles apart producing a measurable impedance change; however, as with other sorption-based detectors, the responses are expected to depend primarily on the equilibrium partition coefficient of the analyte vapor into the sorbant phase [5]. Similarly, the sensitivity of sorption-based polymer film detectors to a given concentration of analyte vapor depends primarily on the vapor pressure of the analyte and only secondarily on more specific chemical interactions between a given analyte and polymer [6]. As a result, for most sorption-based detectors, analyte with low vapor pressures exhibit lower limits of detection (LOD) in general than observed for chemically similar analyte of higher vapor pressures. This trend in sensitivities is echoed in mammalian olfaction [6, 7], with two classes of compounds as notable exceptions [8]. These two classes of analyte, or odorants as they are refereed to in studies of mammalian olfaction, are amines and mercaptans.

The need to quickly and easily ascertain the wholesomeness of foods has forced mammalian olfaction to evolve a specialized strategy for the detection of these two classes of compounds which are present in foods subjected to bacterial decomposition [9-13]. Consequently, the mammalian olfactory system demonstrates much lower LOD for these two types of molecules than for a response dominated primarily by vapor

pressure [7, 8]. In fact, amine and mercaptan gases with vapor pressures much greater than atmospheric pressure are easily detectable to mammals while many other gases lacking these chemical functionalities appear odorless [8]. The mechanism of detection is not well understood, but a separate biological strategy employing receptors that are functionally distinct from those receptors responsible for general olfaction can be predicted for both classes of analyte.

The likely existence of specialized, highly sensitive receptors for amines and mercaptans in mammalian olfactory systems warrants the development of a similarly unique set of detectors in electronic olfaction. Recent work in our laboratory using resistance measurements of polyanaline-carbon black composite films has established LOD on the order of 10 ppt (parts per trillion) for several types of amines [14]. However, a simple, single-element sensor methodology exhibiting enhanced sensitivity for thiols has been lacking from current implementations of the Caltech electronic nose. State-of-the-art detection methods, with both specificity and sensitivity for sulfurous molecules, often require bulky sophisticated instrumentation such as with flame photometric detection [9], and may additionally require that these detectors are coupled to some system for preconcentration of the vapor prior to detection [15, 16]. We present a novel approach for building chemically sensitive resistors from organically capped gold nanocrystals, with both sensitivity and specificity for small mercaptan gases and vapors. This simple and inexpensive method lowers the LOD for molecules such as CH_3SH and H_2S from previous electronic nose detection levels.

Organically capped metal nanocrystals consist of a small metal core (typically less than 10 nm in diameter) surrounded by a dense organic layer [17-21]. These materials are easily synthesized using wet chemistry techniques and remain soluble for extended periods. In either a dry film of nanocrystals or in a concentrated solution, the organic layers serve to separate the metal regions of multiple particles. If the metallic cores of neighboring nanocrystals come into contact, they can fuse, loosing solubility and

eventually transitioning from a soluble material composed of isolatable nanocrystals into an insoluble semi-continuous metal film; consequently, the organic layer surrounding the metal core must remain intact and well ordered to avoid this particle coalescence.

The most commonly used precursor materials for the organic capping layer on noble metal nanocrystals are straight chain alkanethiols [17]. Only a comparatively small amount of work has focused on other organic capping layers such as alkylamines [22, 23]; however, these amine-capped gold nanocrystals are also reportedly stable with respect to coalescence and loss of solubility when stored in solution or as dry powders. The alkylamine at the gold interface is charge neutral, and the robustness of these nanocrystals with respect to the degradative processes leading to particle coalescence has been described as predominantly a kinetic property, rather than a thermodynamic stability [22].

Amine-capped nanocrystals provide a suitable material for a novel type of resistive composite sensor with unique properties The highly conductive gold cores are separated by the electrically insulating organic phase, thus films of nanocrystals exhibit extremely high electrical resistances. Terrill et al. showed that the conductivity, σ, of alkanethiolate stabilized nanocrystals satisfies the following equation over a range of sizes

$$\sigma(T,\delta) = \sigma_o e^{-\delta edge \cdot B} e^{-\Delta G^{\ddagger}/RT} \qquad (1)$$

where δedge is the edge-to-edge metal core separation, B is the electron transfer coupling coefficient, and $\Delta G^{\ddagger}$ is the electron hop activation energy [18]. The conductivity of alkylamine stabilized nanocrystals is similarly expected to decrease exponentially with the thickness of the insulating organic layer. This combination of a strong dependence of the conductivity on the core-to-core separation, and the inherently weak nature of the amine gold interface [22], provides lends this material to the development of a new type of chemically sensitive resistor. Any reaction at the amine core interface that alters the

stability of this material should have a significant effect on a resistance signal. We demonstrate herein, that films of dodecylamine-capped gold nanocrystals are highly sensitive to mercaptan gases and vapors. We propose that small analyte molecules displace and destabilize the protective layer (Scheme I), resulting in a substantial decrease in resistance. Additionally, we show that for exposures of CH_3SH (methylmercaptan), sensors of this type provide a descriptor that is linearly dependant on the concentration of the analyte.

II. EXPERIMENTAL

A. Materials

The solvents, hexanes, acetone, toluene, ethanol (95%), and glacial acetic acid were purchased from EM Science while the reagents sodium borohydride ($NaBH_4$) and dodecylamine and the test analytes propanethiol and octanethiol were purchased from Aldrich Chemical Corp. The gold salt, hydrogen tetrachloroaurate(III) trihydrate ($HAuCl_4 \cdot 3H_2O$), was purchased from Johnson-Mathey. Methylmercaptan (CH_3SH, 958.4 ppm in nitrogen), CH_3SH (10.5 ppm in nitrogen), and Hydrogen Sulfide (H_2S, 1080 ppm in nitrogen) were purchased in cylinders from Matheson. All solvents, reagents, and gases were used as received.

B. Preparation of Gold Nanocrystal Solutions

Alkylamine capped gold nanocrystals were synthesized without the use of a phase transfer reagent according to the procedure developed by Leff et al. [22]. Briefly, 0.42 g hydrogen tetrachloroaurate was dissolved into 100 ml of deionized water in a 2000 ml round bottom flask. A second solution was added to the flask containing 0.62 g dodecylamine dissolved into 100 ml of toluene. This biphasic mixture was stirred vigorously with a 3 cm long magnetic stir bar while a solution of freshly prepared 0.62 g sodium borohydride dissolved in 100 ml of deionized water was added over the course of approximately 90 s. After stirring for 14 h, the organic phase was separated and rinsed three times with 100ml of deionized water in a separatory funnel. The soluble product remaining in the organic phase was filtered through 0.45 μm nylon filter paper and concentrated with rotary evaporation to approximately 4 ml and then precipitated in 800 ml of ethanol at 260 K. This precipitate was then collected on a second 0.45 μm nylon filter paper and redissolved into a small amount of (≈ 20 ml) of hexane. The solution was stored in a freezer until needed.

C. Substrates and Detector Films

Nanocrystal films were prepared on 1 cm x 2 cm glass substrates patterned with a set of electrodes designed for the measurement of highly resistive materials. The IDE (interdigitated electrode) pattern consisted of 50 nm of gold over a 30 nm adhesion layer of chromium, and defined on each substrate 20 parallel sets of lines, 5 mm in length, and separated by 10 μm. The nanocrystal films were cast by manually depositing drops from a hexane solution directly over the electrode region. During the application, the substrates were spun (≈ 700 RPM) on a spin-coater (Headway Research Inc.). The film was allowed to dry briefly (2 or 3 s) between successive drops, and typically 10-15 drops were applied. Because the IDE substrates were made from gold, a control experiment was performed to ensure that the properties of the gold electrodes themselves did not contribute significantly to the responses observed for mercaptan exposures. Briefly, a highly resistive (> 100 kΩ) polyethylene-co-vinyl acetate - carbon black detector was deposited onto an IDE substrate and then exposed to CH_3SH for several minutes. No change in the resistance of the composite detector/IDE was observed, indicating that changes in the electrode itself do not contribute to a significant part of the response observed for these analyte. Control tests with H_2S did in some cases result in a slight drift in the direction of increasing resistance of the electrodes, but these control tests never produced the characteristic response of decreasing resistance described below.

D. Vapor Flow Apparatus

A computer controlled automated flow system (Scheme II) was used to deliver controlled pulses of a diluted stream of an analyte gas or solvent vapor to the detectors [6]. The background air was oil-free air obtained from the house compressed air source (1.10 ± 0.15 parts per thousand (ppth) of water vapor) controlled with a 28 L min^{-1} mass flow controller (UNIT).

1. Vapors derived from liquid sources

To obtain the desired concentration of analyte in the gas phase, a stream of carrier gas controlled by a 60 ml min^{-1} mass flow controller was passed through a bubbler. Saturation of the gas flow through the bubbler of interest was confirmed with a flame ionization detector (Model 300 HFID, California Analytical Instruments, Inc.). The saturated gas stream was then switched in and out of the background stream with a diverting solenoid valve (12V DC Teflon, Cole Parmer), diluting the saturated vapor with background air to produce the desired analyte concentration while maintaining the total air flow at a constant value of either 4 or 5 L min^{-1} during the entire period of an experiment, whether before, during, or after the exposure.

2. Experiments with gaseous analyte

Tanks of H_2S and CH_3SH as mixtures in nitrogen were purchased from Matheson in the following concentrations: CH_3SH 958.4 ppm and 10.5 ppm, and H_2S 1080 ppm. These tanks were connected through a stainless steel pressure regulator to either a 60 ml min^{-1} or 8 ml min^{-1} mass flow controller and then farther diluted with the background air. The analyte gas was switched in and out of the background stream with a diverting solenoid valve, and in all experiments, the total air flow into the sample chamber was held at a constant value of either 4 or 5 L min^{-1} before, during, and after the exposure period. The period of the exposure was adjusted to provide a sufficient response, and ranged from 60 s for high concentrations of analyte to 600 s at low concentrations.

E. DC Resistance Measurements and Data Analysis

1. Measurement setup

Each glass electrode, fabricated pattern, and deposited film of amine capped nanocrystals comprised one sensor. Typically 3 to 6 of these sensors were prepared at a time, and were placed in a row in a small linear chamber constructed of aluminum and Teflon with an internal cross-sectional area of approximately 3 cm^2. The dc resistance of each sensor was measured with a multiplexing digital multimeter (Model HP 34970a,

Hewlett Packard) using short twisted-pair connections and integration times spanning at least two power line cycles. A personal computer running applications developed with LabVIEW 5.0 controlled both the flow system and the data acquisition apparatus. Each sensor was used only once, then discarded.

2. Resistance response data analysis

The magnitude of the electrical resistance of each detector was initially very high (10 kΩ - 100 MΩ) and ranged widely for similarly prepared resisters; consequently, a suitable descriptor was required for interpretation of these differing resistance values. A suitable descriptor was found by taking the natural log of each detectors' resistance, and then fitting a straight line to this data in the region corresponding to the range from 95% to 70% of the initial resistance. This slope was used as the detector descriptor for comparing data from multiple sensors and multiple exposures of CH_3SH. For other analyte, where studies of the concentration dependence of the response were not undertaken, no such descriptor was employed in the analysis. Although all of the detectors exhibited pre-exposure drift, some were notably worse than others and drifted out of measurement range 10 kΩ - 100 MΩ. These detectors were excluded from farther data analysis. Data were processed with a program written in Microsoft Excel Visual Basic.

F. UV-vis Absorbance Spectra

Films for absorbance measurement were prepared by spin coating films of dodecylamine capped gold nanocrystals onto a thin glass microscope coverslip. The absorbance spectra of these substrates were recorded between 400 and 700 nm on a UV-vis diode array spectrophotometer (HP 8452A, Hewlett Packard). After recording the pre-exposure spectra, the substrate was exposed for 20 min to propanethiol vapor in air at a concentration of 164 ppth. After the vapor exposure, the absorbance measurement was repeated.

III. RESULTS and DISCUSSION

A. Optical Properties of Films Exposed to Thiol Vapors

The optical properties of dodecylamine-capped gold nanocrystals before and after exposure to mercaptan vapors were investigated. The absorbance spectra of a thin film of the nanocrystals used in this study is displayed in the dark line of Fig 1. This spectrum, which is characteristic of the plasmon resonance of gold nanocrystals has been observed by many workers [17, 22]. This plasmon resonance depends on the size of the nanocrystals, shifting to longer wavelengths with increasing size. The initial λ_{max} depicted in Fig. 1 is consistent with particles ≥ 7 nm in diameter [22]. The light dashed line in Fig. 1 shows the absorption spectra of the same film after a 20 minute exposure to 160 ppth of propanethiol vapor in air. After this exposure, the λ_{max} has shifted to ~ 605nm. This shift in the plasmon resonance is consistent with the formation of larger particles, or a decrease in the interparticle distances as the gold cores become closer together [24] after exposure to a mercaptan vapor.

B. DC Resistance Responses of Films Exposed to Thiol Vapors

Fig. 2 shows the resistance response of a typical dodecylamine capped gold nanocrystal sensor before during and after a 300 s exposure to CH_3SH at 4 ppb (parts per billion) in air. The resistance drift of the sensor, which is well fit with a straight line in the 600 second period prior to initiating the gas exposure, is extrapolated through the remainder of the chart. Upon exposure to this low concentration of CH_3SH, the sensor responds with a rate of decreasing resistance that is greater than the initial drift. The falling resistance is consistent with a decrease in the edge-to-edge core separation upon exposure to even low concentrations of small molecule mercaptan vapors. This is likely the result of place exchange reactions [25] between the incoming thiol molecule and the loosely bound amine layer. This low level detection for CH_3SH is comparable to the human olfactory threshold displayed in Table 1, and substantially improves the

performance of chemically sensitive resistive detectors over previous strategies relying on carbon black-polymer composites, which exhibit no response to CH_3SH.

The thin film sensors used in this study all exhibited some degree of initial resistance drift, which was primarily in the direction of declining resistance. Although gold nanocrystals are typically synthesized with the phase transfer reagent tetraoctylammonium bromide to facilitate the reaction of the gold salt at the interface between the organic and aqueous phases in the reaction mixture, Leff et al. report that residual phase transfer reagent in the cap region greatly reduces the stability of the material [22]. They also note, that when this phase transfer reagent is excluded from the syntheses, the resulting nanocrystals remain stable for extended periods. The nanocrystals used in this study, although synthesized without phase transfer reagent, showed marked instability when cast into thin films. This instability was characterized by the transformation from soluble to insoluble material and the change from a dark red or purple colored film to a yellow gold color film. The transition was also accompanied by a significant drift in the direction of decreasing resistance. This instability presents a significant limitation to the usefulness of this sensing methodology. Although smaller particles may have exhibited greater stability [19, 21], attempts to use smaller particle films were unsuccessful due to the increased resistance, which exceeded the range of the resistance meter for the electrode geometry employed in this study. Similarly, thicker capping regions may have improved the stability, but this too would increase the resistance significantly. Small quantities of sulfides are present in the atmosphere, which could lead to the sensor drift; however, degradation of the material proceeded similarly even when the sensor chamber was held under a flow of compressed nitrogen.

Fig. 3 shows similar data for a similarly prepared sensor in response to an exposure of CH_3SH at a concentration of 150 ppb in air. The resistance of this sensor fell more rapidly, which is indicative of a greater rate of cap displacement at the higher concentration of analyte. Because the magnitude of the electrical resistance of each

detector was initially very high (10 kΩ - 200 MΩ), and very different for similarly prepared resisters, a suitable descriptor was required for interpretation of the responses. As depicted in Fig. 4, the natural log of each detector resistance was taken, and then a straight line was fit to the region extending from 95% of the initial resistance to 70% of the initial resistance. For sensors with very small responses (< 30%), a smaller region extending from 95% of the initial resistance to 85% of the initial resistance was used. This region was well fit to a straight line for all of the CH_3SH exposures ($R^2 \geq 0.963$) and the slope of this line was used as the response descriptor. The form of the response is consistent with the predicted exponential increase in conductivity upon decreasing edge-to-edge core separations predicted by Eq. (1) [18]. This descriptor worked well for CH_3SH responses, and the result of exposures of 6 different concentrations (0.004, 0.017, 0.150, 0.380, 1.15, and 1.5 ppm) in air are displayed as a function of CH_3SH concentration in Fig. 5. The resulting data was well fit to a straight line with a small intercept indicating that this descriptor provides significant correlation with CH_3SH concentration.

As described above, the optical absorbance was recorded before and after some of these exposures to CH_3SH. This absorbance typically exhibited λ_{max} values that shifted to longer wavelengths. These changes were quite small however, and the electrical resistance change with its large dependence on particle to particle separation provided a more sensitive method of transducing the analyte induced changes in the detector film. Resistance measurement also has the significant advantage of requiring only low cost and low power electronic components, is easily multiplexing, and is compatible with portable devices due to the low profile design of the sensor.

The response of a dodecylamine capped nanocrystal film upon exposure to a longer chain mercaptan, octanethiol, is shown in Fig. 6. This response shows the increasing resistance during and after exposure of a sensor to 600 s of octanethiol vapor at 20 ppm in air. This is consistent with of an increase in the edge-to-edge core

separations upon incorporation of the mercaptan into the film, even though octanethiol is clearly shorter in length than dodecylamine. The responses of several sensors to octanethiol, although all positive and persistent after ending the exposure, were varied and did not easily lend themselves to analysis.

The response of the detector to another gas, H_2S at 8.6 ppm in air, is displayed in Fig. 7. The responses of the detectors to H_2S were varied. Only 3 of the 6 detectors studied at this analyte concentration exhibited the characteristic response in Fig. 7. Some showed slight initial increases in resistance followed by decreasing resistance, and others did not respond significantly. Although this level is well above the human olfactory threshold, it may be useful in environmental monitoring because it is lower than the recommended maximum workplace value for this gas [26] shown in Table 1.

An important property of these sensors beyond their sensitivity is their specificity to mercaptan vapors. Films of dodecylamine nanocrystals did not produce the characteristic decreasing resistance responses of Figs. 2, 3, and 7 upon exposure to common (non-mercaptan) solvents and vapors. Only small positive increases in resistance were observed for exposures of water and common organic solvents, which is consistent with the operating principle reported previously for alkanethiolate-capped gold nanocrystal sensors [4]. As shown in Fig. 8, in consecutive 120 s exposures to acetone and toluene at concentrations of 12 and 1.5 ppth, respectively, the sensor resistance increased only slightly and reversibly in each exposure. However, when exposed to a harsh vapor such as acetic acid at a concentration of 0.80 ppth, the sensor did exhibit at least some decrease in resistance following an initial resistance spike. This may be consistent with the sorption of this carboxylic acid into the film, producing a slight swelling-type response, followed by the reaction of the acid with the amine, causing a decreased stability of the capping layer.

IV. CONCLUSIONS

The electrical resistance of dodecylamine-capped gold nanocrystal films on IDEs exhibits a significant change upon exposure to CH_3SH gas. This reaction is well fit, and the rate of this reaction under a given set of experimental conditions is dependent on the concentration of the CH_3SH. This method of detection provides linear responses to CH_3SH between 0.153 and 1.53 ppm ($R^2 = 0.9882$), although responses were visible at the lowest concentrations tested of 1.6 ppb. The detector films also exhibited similar responses to H_2S at concentrations as low as 1.4 ppm although the form of this response was more complicated and less robust. The addition of such a sensor to an array of nonspecific vapor detectors extends the capability of the array to the detection of small mercaptan gases undetectable with previous implementations of the electronic nose.

V. ACKNOWLEDGEMENTS

We acknowledge NASA, DOE, the NIH, and an Army MURI for their generous support of this work.

VI. TABLES

Table 1: Standardized Human Olfactory Thresholds and Maximum Workplace Concentrations

	Compound	Odor Threshold Value (ppb)	Maximum Concentration Value in the Workplace [a] (ppb)
mercaptans	H_2S	18	10^4
	CH_3SH	1.0	$5x10^2$
	$(CH_3)_2S$	0.6-40 [a]	$2x10^4$
	propane-SH	1.3	-
alcohols	CH_3OH	$1.4x10^5$	-
	propane-OH	$2.4x10^3$	-

[a] Values are taken from [26]. All other values are from [8].

VII. SCHEMES AND FIGURES

Scheme 1. A proposed mechanism for the resistance and optical changes incurred by thin films of dodecyl amine capped gold nanocrystals upon exposure to vapors possessing the thiol (-SH) functionality.

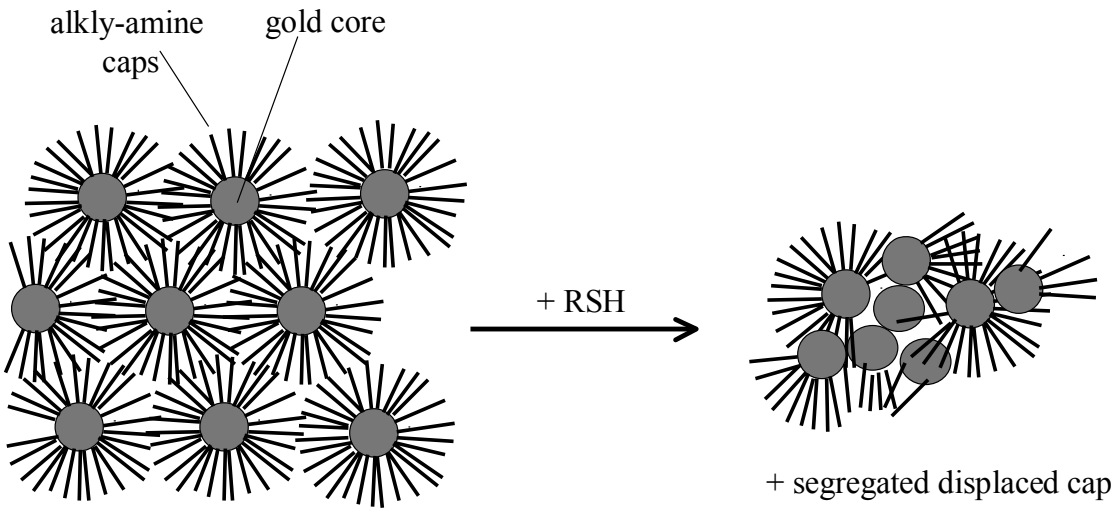

Scheme 2. A layout of the automated experimental system used to control gas and liquid vapor exposures. The system was coupled with a multiplexed resistance read-out system, which is also shown.

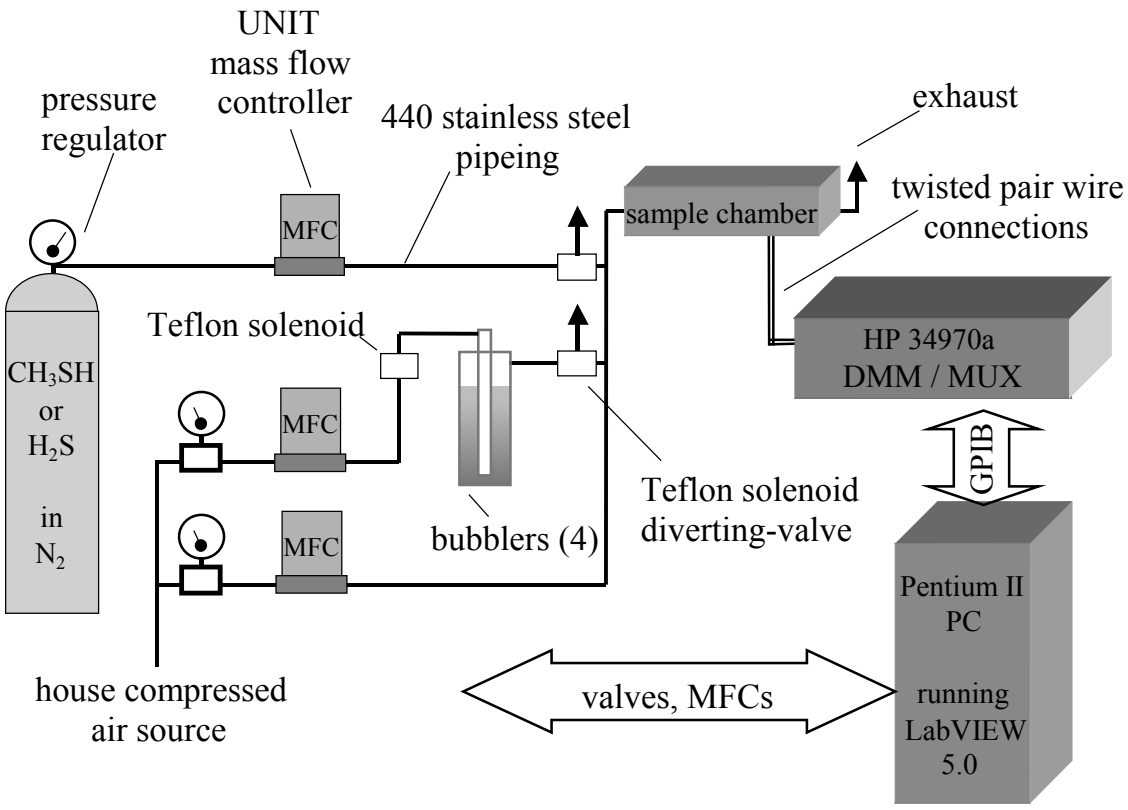

Fig. 1. UV-vis absorbance spectra from 400 to 700 nm acquired for a thin film of dodecyl-amine capped gold nanocrystals on a glass microscope coverslip. The dark line indicates the absorbance spectra of the red film before exposure with λ_{max} of 565 nm, and the light dashed line indicates the spectra after exposure to 160 ppth propanethiol vapor in air for 20 min. After exposure, the film was notably blue in color with λ_{max} of 605 nm.

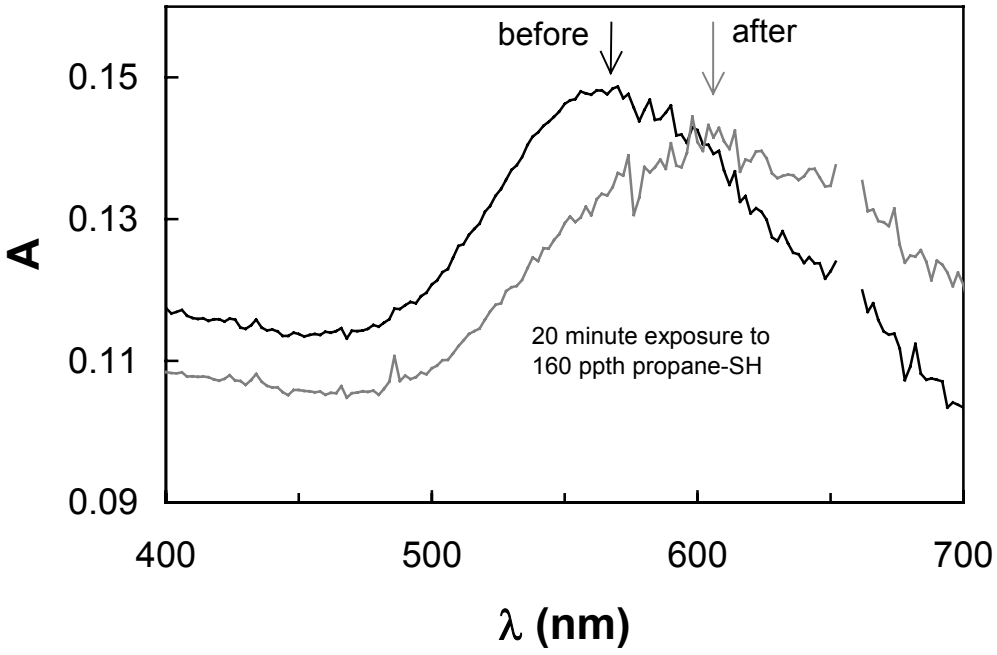

Fig. 2. A plot of resistance (black) vs. time for a typical dodecylamine nanocrystal film (this detector was located in the third position of the sample chamber with respect to the source of the vapor). For the first 300 s, laboratory air at 5.0 L min^{-1} was delivered across the detectors in the sample chamber, then starting at time zero and continuing for a period of 300 s, laboratory air spiked with CH_3SH at a concentration of 4 ppb was delivered through the detector chamber at 5.0 L min^{-1}. After the exposure, analyte-free laboratory at a flow rate of 5.0 L min^{-1} was blown through the chamber for an additional 300 s. This detector was exposed once then discarded. The dashed line (gray) shows the drift for the sensor extrapolated over the time of the experiment. This line was fit from -600 to 0 s (first 300 s not shown), with a slope of -4 kΩ s^{-1} (R^2=0.9998).

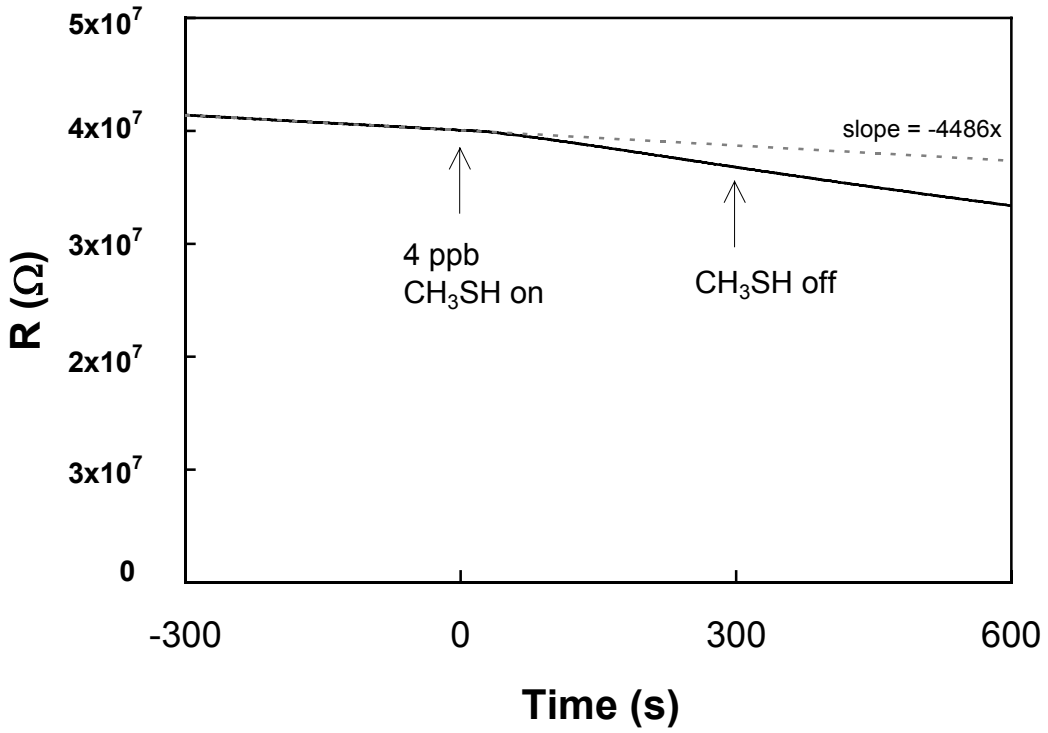

Fig. 3. A plot of resistance vs. time (black) for a typical dodecylamine nanocrystal film (this detector was located in the third position of the sample chamber with respect to the source of the vapor). For the first 300 s, laboratory air at 5.0 L min^{-1} was delivered across the detectors in the sample chamber, then starting at time zero and continuing for a period of 300 s, laboratory air spiked with CH_3SH at a concentration of 150 ppb was blown through the detector chamber at 5.0 L min^{-1}. After the exposure, analyte-free laboratory at a flow rate of 5.0 L min^{-1} was delivered through the chamber for an additional 300 s. This detector was exposed once then discarded. The dashed line (gray) shows the drift for the sensor extrapolated over the time of the experiment. This line was fit from -600 to 0 s (first 300 s not shown), with a slope of -3 kΩ s^{-1} (R^2=0.9998).

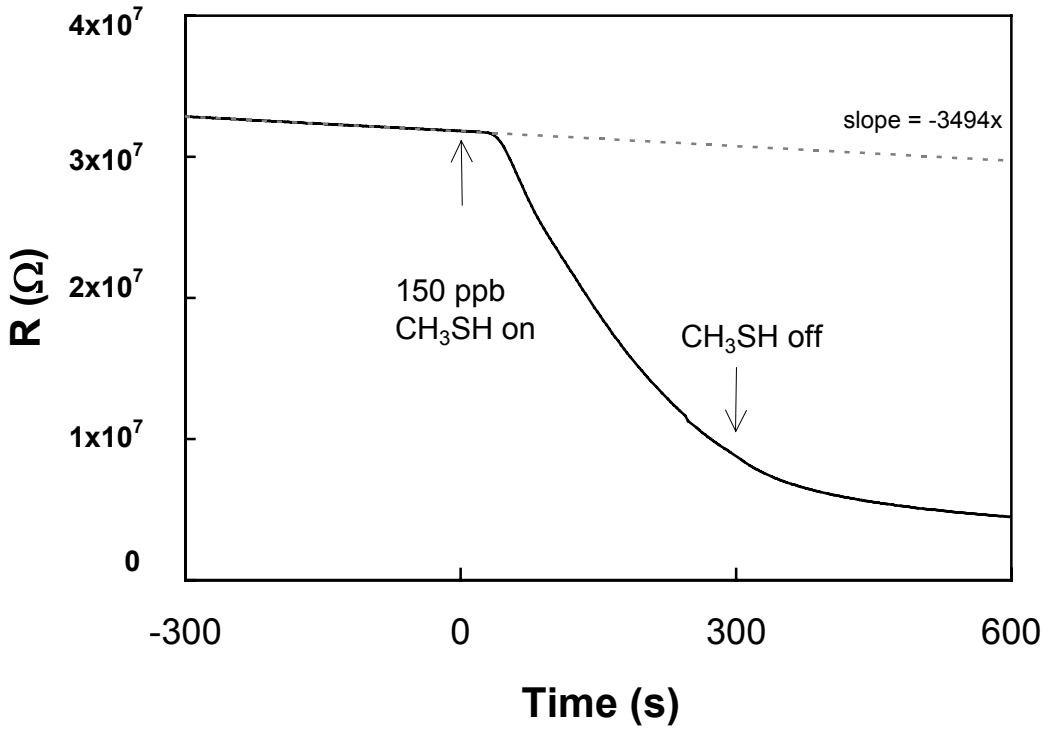

Fig. 4. A plot of the natural log of resistance vs. time for the data presented in Fig. 3. The natural log of the response was well fit to a straight line with a slope of -0.0047 s^{-1} (R^2=0.9987). The slope, fit from the region of 95% to 70% of the maximum resistance, was used as the response descriptor.

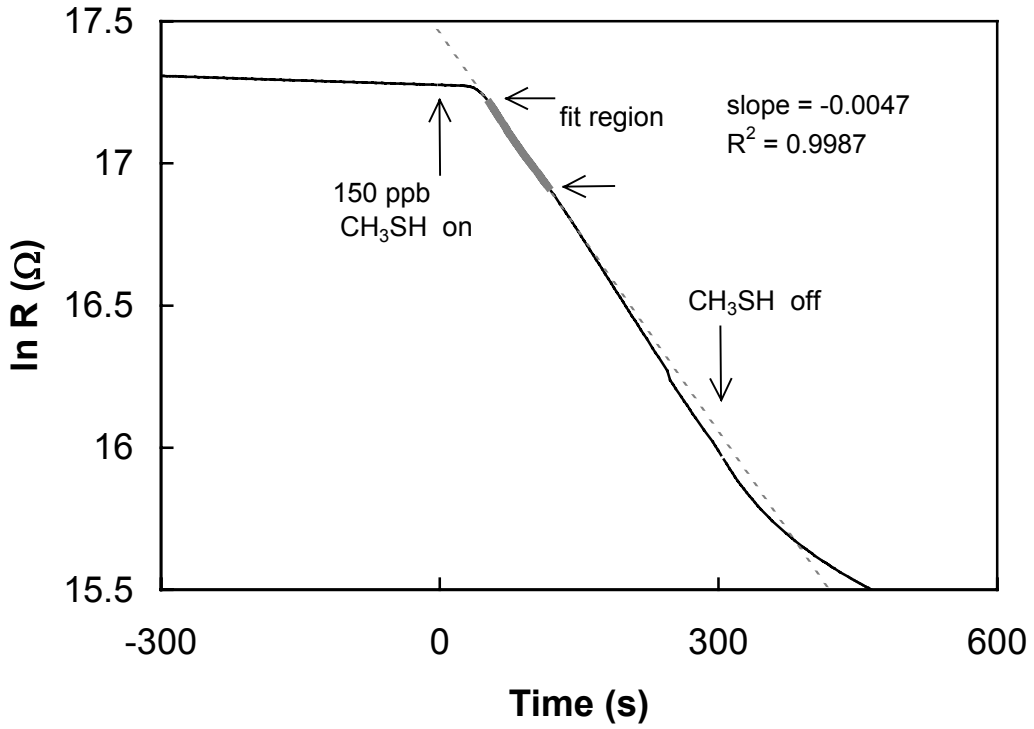

Fig. 5. A plot of the response descriptor (slope of ln R between 95% and 75% of each detectors initial resistance) upon exposure to various concentrations of CH_3SH. Each data point (cross) is the average of three separate detectors for each of six concentrations of the mercaptan (0.004, 0.017, 0.150, 0.380, 1.15, and 1.5 ppm) in air. The data was fit with a straight line (dashed gray) with a slope of -0.0225 s^{-1} ppm^{-1} and an intercept of -0.0018 ppm (R^2 = 0.9882). The 18 detectors represented by this figure were each exposed only once and then discarded.

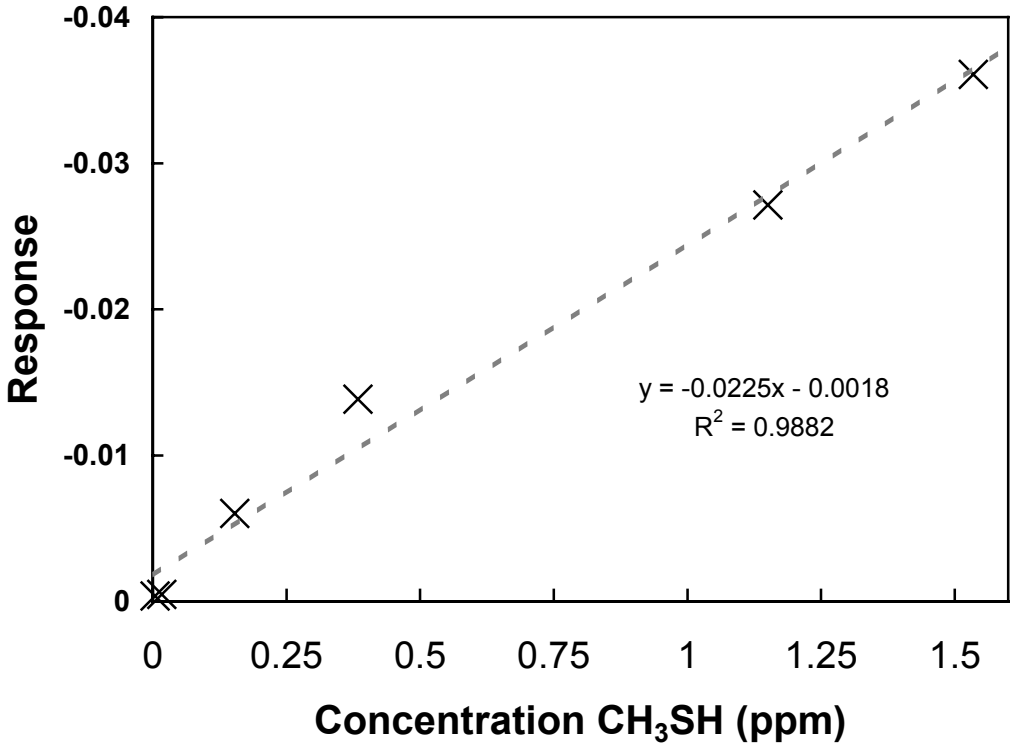

Fig. 6. A plot of resistance vs. time (black) for a typical dodecylamine nanocrystal thin film detector (this detector was located in the third position of the sample chamber with respect to the source of the vapor). For the first 300 s, laboratory air at 5.0 L min^{-1} was directed across the detectors in the sample chamber, then starting at time zero and continuing for a period of 600 s, laboratory air spiked with octanethiol (octane-SH) at a concentration of 20 ppm was blown through the detector chamber at 5.0 L min^{-1}. After the exposure, analyte-free laboratory at a flow rate of 5.0 L min^{-1} was directed through the chamber for an additional 300 s. This detector was exposed once then discarded. The dashed gray line indicates the drift for the sensor extrapolated over the time of the experiment. The drift line was fit from -600 to 0 s (first 300 s not shown), with a slope of -39 Ω s^{-1} (R^2=0.9986).

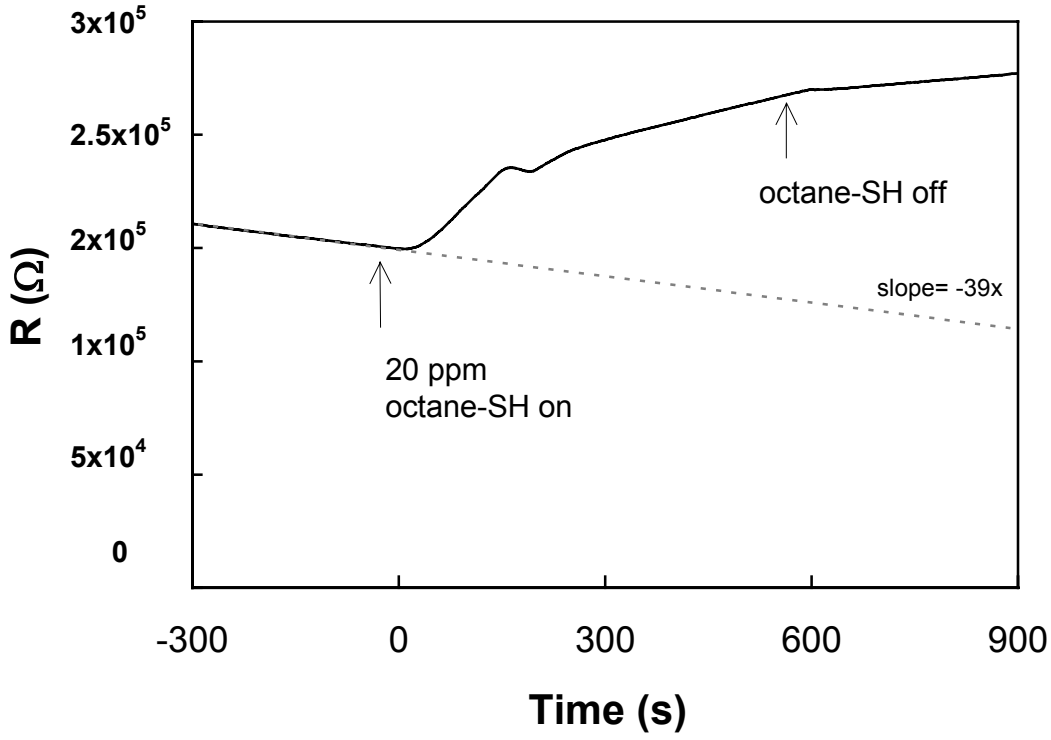

Fig. 7. A plot of resistance vs. time (black) for a dodecylamine nanocrystal thin film detector (this detector was located in the fourth position of the sample chamber with respect to the source of the vapor because the detector in the third position exhibited no response). For the first 300 s, laboratory air at 5.0 L min^{-1} was directed across the detectors in the sample chamber, then starting at time zero and continuing for a period of 300 s, laboratory air spiked with H_2S at a concentration of 8.6 ppm was directed through the detector chamber at 5.0 L min^{-1}. After the exposure, analyte free laboratory at a flow rate of 5.0 L min^{-1} was directed through the chamber for an additional 300 s. This detector was exposed once then discarded. The dashed line (gray) shows the drift for the sensor extrapolated over the time of the experiment. This drift line was fit from -600 to 0 s (first 300 s not shown), with a slope of -680 Ω s^{-1} (R^2=0.9996).

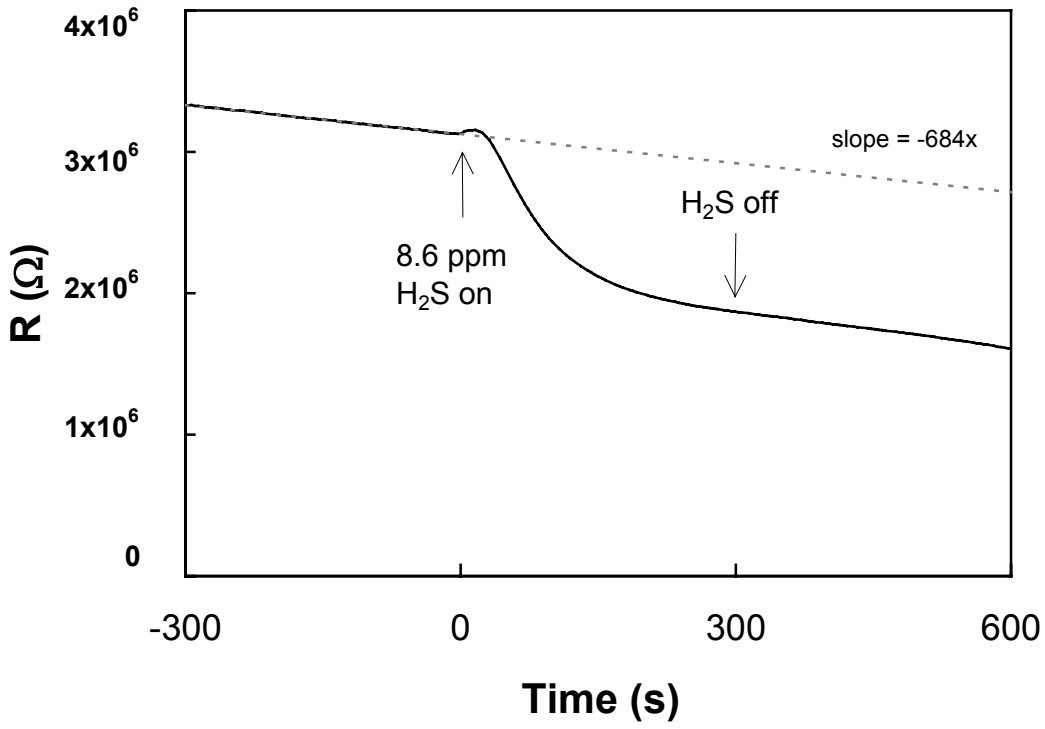

Fig. 8. A plot of resistance vs. time for a dodecylamine-capped gold nanocrystal thin film detector. At 720 s, and continuing for a period of 120 s, laboratory air spiked with acetone vapor at a concentration of 12 ppth was directed through the detector chamber at 4.0 L min^{-1}. At 1080 s, and continuing for a period of 120 s, laboratory air spiked with toluene vapor at a concentration of 1.5 ppth was directed through the detector chamber at 4.0 L min^{-1}. At 1440 s, and continuing for a period of 120 s, laboratory air spiked with acetic acid vapor at a concentration of approximately 0.80 ppth was directed through the detector chamber at 4.0 L min^{-1}. Before the first exposure, in the time periods between the three exposures, and after the last exposure, analyte-free laboratory air was directed through the detector chamber at a flow rate of 4.0 L min^{-1}.

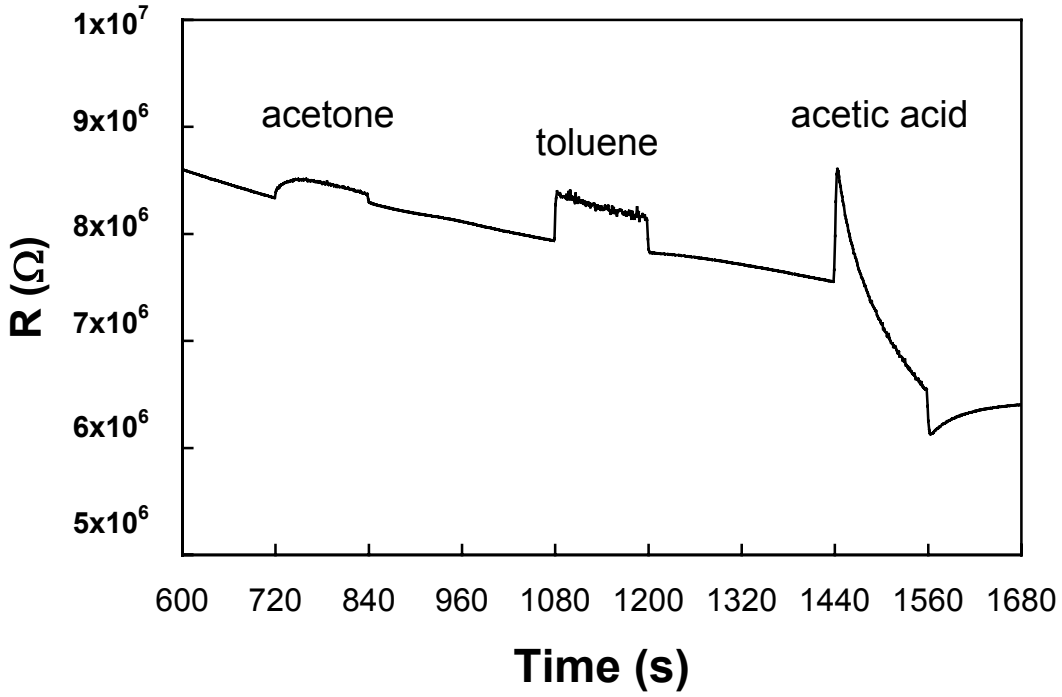

VIII. REFERENCES

1. K. C. Persaud, G. H. Dodd, Nature, 299 (1982) pp. 352
2. I. Lundstrom, M. S. Shivaraman, C. S. Svenson, L. Lundkvist, Appl. Phys. Lett. 26 (1975) pp. 55
3. T. Vossmeyer, B. Guse, I. Besnard, R. E. Bauer, K. Mullen, A. Yasuda, Gold nanoparticle/polyphenylene dendrimer composite films: Preparation and vapor-sensing properties, Adv. Mater. 14 (2002) pp. 238
4. H. Wohltjen, A. W. Snow, Colloidal metal-insulator-metal ensemble chemiresistor sensor, Anal. Chem. 70 (1998) pp. 2856-2859
5. G. Harsanyi. *Polymer Films in Sensor Applications*, Technomic, Lancaster, 1995.
6. B. J. Doleman, E. J. Severin, N. S. Lewis, Trends in odor intensity for human and electronic noses: Relative roles of odorant vapor pressure vs. molecularly specific odorant binding, Proc. Natl. Acad. Sci. U.S.A. 95 (1998) pp. 5442-5447
7. B. J. Doleman, N. S. Lewis, Comparison of odor detection thresholds and odor discriminablities of a conducting polymer composite electronic nose versus mammalian olfaction, Sens. Actuator B-Chem. 72 (2001) pp. 41-50
8. M. Devos, Patte, F., Rouault, J., Laffort, P. and Van Gemert, L.J. *Standardized Human Olfactory Thresholds*, Oxford University Press, New York, 1990.
9. P. G. Hill, R. M. Smith, Determination of sulphur compounds in beer using headspace solid-phase microextraction and gas chromatographic analysis with pulsed flame photometric detection, J. Chromatogr. A 872 (2000) pp. 203-213
10. J. E. Stratton, R. W. Hutkins, S. L. Taylor, Biogenic-amines in cheese and other fermented foods: A review, J. Food Prot. 54 (1991) pp. 460-470
11. A. R. Shalaby, Significance of biogenic amines to food safety and human health, Food Res. Int. 29 (1996) pp. 675-690

12. S. C. Su, S. S. Chou, P. C. Chang, D. F. Hwang, Determination of biogenic amines in fish implicated in food poisoning by micellar electrokinetic capillary chromatography, J. Chromatogr. B 749 (2000) pp. 163-169

13. M. Mestres, M. Marti, O. Busto, J. Guasch, Simultaneous analysis of thiols, sulphides and disulphides in wine aroma by headspace solid-phase microextraction-gas chromatography, J. Chromatogr. A 849 (1999) pp. 293-297

14. G. A. Sotzing, J. N. Phend, R. H. Grubbs, N. S. Lewis, Highly sensitive detection and discrimination of biogenic amines utilizing arrays of polyaniline/carbon black composite vapor detectors, Chem. Mat. 12 (2000) pp. 593-595

15. R. A. Murray, Limitations to the use of solid-phase microextraction for quantitation of mixtures of volatile organic sulfur compounds, Anal. Chem. 73 (2001) pp. 1646-1649

16. A. Tangerman, Determination of volatile sulfur-compounds in air at the parts-per-trillion level by tenax trapping and gas-chromatography, Journal of Chromatography 366 (1986) pp. 205-216

17. M. Brust, M. Walker, D. Bethell, D. J. Schiffrin, R. Whyman, Synthesis of thiol-derivatized gold nanoparticles in a 2-phase liquid-liquid system, J. Chem. Soc.-Chem. Commun. (1994) pp. 801-802

18. R. H. Terrill, T. A. Postlethwaite, C. H. Chen, C. D. Poon, A. Terzis, A. D. Chen, J. E. Hutchison, M. R. Clark, G. Wignall, J. D. Londono, R. Superfine, M. Falvo, C. S. Johnson, E. T. Samulski, R. W. Murray, Monolayers in three dimensions: NMR, SAXS, thermal, and electron hopping studies of alkanethiol stabilized gold clusters, J. Am. Chem. Soc. 117 (1995) pp. 12537-12548

19. D. V. Leff, P. C. Ohara, J. R. Heath, W. M. Gelbart, Thermodynamic control of gold nanocrystal size: Experiment and theory, J. Phys. Chem. 99 (1995) pp. 7036-7041

20. S. J. Green, J. J. Stokes, M. J. Hostetler, J. Pietron, R. W. Murray, Three-dimensional monolayers: Nanometer-sized electrodes of alkanethiolate-stabilized gold cluster molecules, J. Phys. Chem. B 101 (1997) pp. 2663-2668

21. M. J. Hostetler, J. E. Wingate, C. J. Zhong, J. E. Harris, R. W. Vachet, M. R. Clark, J. D. Londono, S. J. Green, J. J. Stokes, G. D. Wignall, G. L. Glish, M. D. Porter, N. D. Evans, R. W. Murray, Alkanethiolate gold cluster molecules with core diameters from 1.5 to 5.2 nm: Core and monolayer properties as a function of core size, Langmuir 14 (1998) pp. 17-30

22. D. V. Leff, L. Brandt, J. R. Heath, Synthesis and characterization of hydrophobic, organically soluble gold nanocrystals functionalized with primary amines, Langmuir 12 (1996) pp. 4723-4730

23. M. Green, N. Allsop, G. Wakefield, P. J. Dobson, J. L. Hutchison, Trialkylphosphine oxide/amine stabilized silver nanocrystals: the importance of steric factors and lewis basicity in capping agents, J. Mater. Chem. 12 (2002) pp. 2671-2674

24. R. Elghanian, J. J. Storhoff, R. C. Mucic, R. L. Letsinger, C. A. Mirkin, Selective colorimetric detection of polynucleotides based on the distance-dependent optical properties of gold nanoparticles, Science 277 (1997) pp. 1078-1081

25. M. J. Hostetler, A. C. Templeton, R. W. Murray, Dynamics of place-exchange reactions on monolayer-protected gold cluster molecules, Langmuir 15 (1999) pp. 3782-3789

26. E. Smet, P. Lens, H. Van Langenhove, Treatment of waste gases contaminated with odorous sulfur compounds, Crit. Rev. Environ. Sci. Technol. 28 (1998) pp. 89-117